IOSR Journal of Nursing and Health Science (IOSR-JNHS)
e-ISSN: 2320–1959.p- ISSN: 2320–1940 Volume 15, Issue 2 Ser. 3 (Mar. – Apr. 2026), PP 13-22
www.iosrjournals.org

Performance Characteristics Of LYSO Scintillation Crystals Based On 15cm (3 Ring) TOF PET/CT

Rasool Kattubadi, Elmubarak Mohamedahmed, Hamad Almajid
Medical Physicist, Nuclear Medicine Unit, Medical Imaging Department, King Abdul-Aziz Medical City Riyadh. Consultant Medical Physicist Medical Physics Unit, Medical Imaging Department, King Abdul-Aziz Medical City Riyadh,
Medical Physicist, Nuclear Medicine Unit, Medical Imaging Department, King Abdul-Aziz Medical City Riyadh

Abstract
Background: *This paper represents the National Electrical Manufacturers Association (NEMA) system performance of the Discovery MI 3-ring PET/CT (GE Healthcare) installed in advanced cardiac unit, King Abdulaziz Hospital (KAH), Advanced cardiac unit, Riyadh. This time-of-flight (TOF) PET camera is based on lutetium-based scintillation crystals. LYSO, Lutetium–yttrium oxyorthosilicate is an inorganic chemical compound with main use as a scintillator crystal for gamma radiation detection.*
Methods: *The NEMA NU2-2018 standard was used to evaluate spatial resolution, sensitivity, image quality (IQ) and count rate curves of the system. Timing and energy resolution were determined.*
Results: *Full width at half maximum (FWHM) of spatial resolution in radial, tangential and axial direction was 3.84, 3.84 and 4.18 mm at 1 cm; 4.66, 4.08 and 4.91 mm at 10 cm; and 7.15, 5.31 and 5.47 mm at 20 cm from the centre of the field of view (FOV) for the VPHD reconstruction. For non-TOF ordered subset expectation maximization (OSEM) reconstruction without point spread function (PSF) correction, FWHM was 3.87, 3.69 and 4.15 mm at 1 cm; 4.80, 3.81 and 4.87 mm at 10 cm; and 7.38, 4.16 and 3.98 mm at 20 cm. Sensitivity was 7.12 cps/kBq at the centre of the FOV and 6.84 cps/kBq at 10-cm radial offset. Contrast recovery (CR) using the IQ phantom for the TOF VPFX reconstruction was 105.3, 119.7, 126.8 and 98.1% for the 10-, 13-, 17- and 22-mm radioactive spheres and 96.5 and 92.2% for the 28- and 37-mm non-radioactive spheres. Background variability (BV) was 17.5, 12.7, 9.0, 7.1, 5.5 and 4.5% for the 10-, 13-, 17-, 22-, 28- and 37-mm spheres. Lung error was 7.8%. Peak noise equivalent count rate (NECR) was 114.3 kcps at 22.20 kBq/ml with a scatter fraction of 42.10%. Maximum accuracy error was 3.88%. Coincidence timing resolution at 5.3 kBq/ml was 411.2 ps FWHM. Energy resolution was 9.94% FWHM. Observed that Q.Clear reconstruction significantly improved CR and reduced BV compared with OSEM while processing the data.*
Conclusion: *System sensitivity and NECR are lower and IQ phantom's BV is higher compared with larger axial FOV (AFOV) scanners like the 4-ring discovery MI, as expected from the smaller solid angle of the 3-ring system. The other NEMA performance parameters are all comparable with those of the larger AFOV scanners.*
Keywords: *Lutetium based PET/CT, NEMA, Discovery MI 3-ring, Time-of-flight PET/CT*

Date of Submission: 19-04-2026 Date of Acceptance: 29-04-2026

I. Introduction

Over the past few years, positron-emission tomography (PET) has benefited enormously from various developments, including time-of-flight (TOF), point spread function (PSF) correction and the introduction of solid-state photomultipliers instead of vacuum photomultiplier tubes. Several manufacturers have now brought solid-state photomultiplier-based systems onto the market with hopes of higher image quality and/or lower radiopharmaceutical dose and improved small lesion detection.

In this article, we evaluated the system performance of the Discovery Meaningful Insights PET/CT with a 3-ring PET (Discovery MI 3, GE Healthcare, KAH, Riyadh, KSA) and compared with data on the similar system with Discovery 690/710, which had been performed before. IQ, Decay, CTC data comparison also performed with 4ring system from other hospital.

The 3-ring configuration provides a 15-cm axial field of view. Each PET-ring is made of 34 units consisting of 4 blocks. Every block has 9 (in the axial direction) × 4 (in the in-plane direction) lutetium-yttrium-oxyorthosilicate crystals, for a total of 14,688 crystals for the system. Each crystal element has a dimension of 3.95 mm (transaxial) × 5.3 mm (axial) × 25 mm (length). Each block is coupled with 6 (in the axial direction) × 3 (in the in-plane direction) silicon photomultiplier arrays (SiPM). The Hamamatsu SiPM array has an active area of 4 × 6 mm and is divided into 2 × 3 pixels. The National Electrical Manufacturers Association (NEMA) NU2-2018 standards were used for the evaluation, as in most of the recent literature. Additional measurements were performed according to NEMA NU2-2018 standards.

Reconstruction software available on the Discovery MI 3 system includes filtered backprojection (FBP) and Vue Point FX (VPFX), Vue Point HD (VPHD), an ordered subset expectation maximization (OSEM) algorithm, which can be combined with PSF correction (VPHD-S). The system also has a TOF ability; Vue Point FX (VPFX) refers to the combination of VPHD with TOF.

With conventional iterative reconstruction algorithms based on maximum likelihood estimation maximization, such as OSEM, quantitative accuracy improves with an increasing number of iterations. To prevent excessive noise propagation, the iterations can be stopped before full convergence, but at the expense of lesser quantitative accuracy. Alternatively, the objective function can be extended with a prior favoring smooth solutions and such algorithms can achieve global convergence while retaining fast initial convergence speed. Q.Clear, a Bayesian penalized likelihood technique, uses a relative difference penalty which is a function of the difference between neighboring voxels as well as a function of their sum. The penalty acts to sup- press noise while preserving edges and is modulated by a penalization factor called beta that can be adapted to the data at hand. In each iteration step, the outcomes with lower variation between neighbouring voxels are favoured over the noisier ones. The use of this penalty function thereby allows full convergence, providing more accurate quantitation.

II. Materials And Methods:

NEMA test procedures for Discovery MI were used to perform Scanner Acceptance Testing. Almost all measurements were evaluated per *NEMA Standards Publication NU2-2018.* We made use of the NEMA processing tools contained in the Discovery MI software. Some additional measurements were performed according to NEMA NU2-2018. Before NEMA testing, a normalization scan and well counter calibration were performed. Additional timing resolution and energy resolution tests were performed.

Normalization and well counter correction:

A normalization scan was performed before the NEMA tests started. We used the calibration/daily quality assurance phantom, which is a 27.6-cm long, 12.5-cm outer diameter (1.3-cm thick) annulus phantom filled with ^{68}Ge radioactive source an epoxy matrix (1260mL). Normalization was performed using Ge68 DQA Annulus phantom 18.5 MBq (1.49mCi) (activity concentration at time of acquisition). This phantom is provided with the scanner for calibrations and daily quality assurance. A well counter calibration was performed with 18.5 MBq (500μCi) (at the start of the acquisition) of ^{18}F-Fluorodeoxyglucose (^{18}F-FDG) in a uniform cylindrical phantom with a diameter of 20 cm and a length of 18 cm. This process provided a normalization sinogram and the activity correction factor [1].

Spatial resolution

^{18}F-FDG was mixed with a small amount of dye to enhance the visibility of the radio- active liquid. Little drops were suspended on a plate and drawn up by capillary tubes so that the axial length of the drop in the tubes was less than 1 mm. Three-point sources were made and inserted in the spatial resolution phantom. The sources were positioned at 1, 10 and 20 cm in the *Y*-direction from the centre of the field of view (FOV). Their positions were adjusted to within ± 1.0 mm of the corresponding nominal positions in the PET's scan FOV. Data were collected at the centre slice of the FOV and at one eighth from the edge of the axial FOV. Every acquisition consisted of at least 500.000 counts. For NEMA, the images were reconstructed with FBP and VPHD, non-TOF OSEM reconstruction with 34 subsets and 4 iterations without PSF modelling. An additional reconstruction was made using VPHD-S. For each spatial orientation, full width at half maximum (FWHM) and full width at tenth maximum (FWTM) were calculated for every reconstruction and every point source and averaged for the acquisition at the centre of the FOV and at 1/8th axial FOV. FWHM and FWTM were statistically compared between the 3 reconstruction algorithms[2].

Sensitivity

A plastic tube (70-cm long and with a lumen of 1 mm) was filled with 14.65 MBq (396μCi) of ^{18}F-FDG at time of filling. The activity was left to decay until it was lower than 4 MBq, in order for count losses to be negligible and random coincidences to be low. With the aid of a dedicated source holder and dedicated software, this line source was placed at the centre of the FOV and at a 10-cm radial offset from isocenter[13].. At each position, 5 1-min scans were made with the number of aluminium sleeves around the plastic tube ranging from 1 to 5. The aluminium ensures the annihilation of all positrons and provides increasing attenuating material. Results were then extrapolated to give the scanner sensitivity with no attenuation material. Data were collected directly from sinograms corrected for randoms. Randoms were subtracted from prompts to obtain trues-only sensitivity results [2].

Scatter fraction, count losses and Randoms

This test measures the count rate performance of the scanner across a range of radio- activity levels. The scatter fraction portion of this test measures the sensitivity of the scanner to coincidence events caused by scatter.

A 70-cm-long line source with an inner diameter of 3.2 mm containing 850 MBq (23 mCi) ^{18}F-FDG at the start of the acquisition was placed in the NEMA scatter phantom, a 70-cm-long polyethylene cylinder with a diameter of 20 cm. The activity was high enough to achieve count rates beyond the expected peak of the noise equivalent count rate. The phantom was secured from rolling with rubber foam wedges and elevated with a paper stack over the patient table until its centre-line aligned with the scanner's central axis. The acquisition started with 17 frames of 15 min, without delay between the frames, and ended with 7 frames of 25 min, each with a delay of 25 min. NEMA specifications were used to derive the trues, randoms, scatter and noise-equivalent count rate (NECR) from the prompts dataset in each frame. Randoms were estimated using singles rates and the coincidence timing window that is defined by the manufacturer for clinical use[18]..

Quantitation accuracy: corrections for count losses and Randoms

This test compares the trues rate inferred from count losses and randoms corrections with the trues rate extrapolated from measurements with negligible count losses and randoms. Calculations were done on the data acquired for the test of scatter fraction, count losses and randoms as described above, reconstructed by non-TOF OSEM with 16 subsets and 3 iterations without point-spread function modelling. In each time frame, the absolute value of the error was calculated from a linear fit of the activity concentrations measured below peak NECR using 41 of the 53 slices comprising the phantom volume (the 6 end-slices were ignored); the mean, maximum and minimum error over these 41 slices were derived. The accuracy of the corrections for count losses and randoms was expressed as the maximal absolute value of the error below peak NECR.

Image quality, attenuation accuracy and scatter correction

The image quality (IQ) test simulates a PET/CT whole body clinical case. The 6 spheres of the IQ phantom with a diameter of 10, 13, 17 22, 28 and 37 mm were filled with 21 kBq/cc (0.567μCi/cc) ^{18}F-FDG, called as hot spheres. The background of the phantom was filled with 5.27 kBq/cc (0.14μCi/cc) ^{18}F-FDG, in order to yield a 4:1 concentration ratio between the radioactive spheres and the background volume. The phantom has a cylindrical insert with a diameter of 5 cm, containing a low-density material with an average density of 0.3 g/ml to simulate lung tissue. This insert is positioned in the centre of the phantom to have a non-uniform background [18]. The IQ phantom was centred in the scan FOV. Additional activity (120 MBq) was placed outside the FOV (70-cm-long line source with ^{18}F-FDG in the NEMA scatter phantom) to represent scatter radiation. Three acquisitions (with time correction for radioactive decay) were made and reconstructed with the VPFX reconstruction algorithm using a 384 × 384 matrix, CT attenuation cor- rection, 4 iterations, 34 subsets, corrections for randoms, scatter, dead time and normalization. IQ was reported in terms of contrast recovery (CR) and background variability (BV) for the radioactive and non-radioactive spheres and averaged over the three acquisitions for increased reliability. The lung error (LE) is the average of LE from 48 slices out of the 53 slices in the PET image, per [4].

The same acquisitions were reconstructed with the VPFX, VPHD reconstruction including Q.Clear reconstruction algorithm, with a beta value of 50. This low beta value, the same that was used in [3], was selected with the intent of matching the noise levels in the Q.Clear and VPFX images. CR and BV were compared between VPFX and Q.Clear reconstructions by paired *t* tests.

An additional acquisition was performed according to NEMA NU2-2018. The 6 spheres of the IQ phantom were now filled with 21.9 kBq/cc ^{18}F-FDG concentration, whereas the background was filled with 5.5 kBq/cc ^{18}F-FDG concentration, again yielding a 4:1 concentration ratio between the radioactive spheres and the background. Phantom positioning and image reconstruction were identical to those described above for the NEMA NU2-2018 testing. An offline analysis tool was used to derive CR and BV values[13]..

Timing and energy resolution

Timing resolution was calculated from the acquisition of a line source filled with 16 MBq (0.405mCi) of ^{18}F-FDG and suspended in the centre of the FOV in the axial direction in the smallest aluminium sleeve used in the NEMA sensitivity test. Energy resolution was calculated from an acquisition with a 55MBq (1.48mCi) ^{68}Ge annular phantom (the scanner's calibration phantom). Three hundred million counts were taken to acquire the timing spectrum. Measurement of the timing resolution FWHM was

based on a 3-point fit of the peak of the timing spectra for each crystal pair after removal of the randoms. The energy spectra were smoothed with a boxcar filter. The timing and energy resolution were calculated for every detector crystal and averaged for the entire system.

PET/CT Co-registration accuracy

According to NEMA NU2-2018, a PET/CT co-registration accuracy scan was performed to analyze the registration between the PET and the CT image. An 4-min single-bed-position PET scan was acquired after CT scan with 50cm DFOV. 55MBq (1.48 mCi) of Fluorodeoxyglucose (18F-FDG) mixed with CT contrast solution (i.e. Iopromide or Ioxitalamic Acid) and filled in 3 spheres with total 20ml volume. IEC (NEMA IQ) phantom hollow spheres 17mm,22mm and 28mm and Spheres position in co-registration holder: 17mm sphere at position (0,1), 22mm sphere at position (0,20), and 28mm sphere at position (20,0). Two scans were performed by positioning the phantom holder on the cradle at 5 ± 2 cm from the tip and holder on the cradle at 100 ± 2 cm from the tip. The total activity in the spheres should be between 40MBq and 60MBq, to produce no more than 5% randoms, but sufficient to produce measurable results. Images were reconstructed using VPFX, in a 384 × 384 matrix, with 3subsets and 4 iterations and using a standard Z axis filter with 2.0-mm filter cutoff. Dedicated software was used to determine the coordinates of every point source on both PET and CT images. The difference between the PET and CT coordinates along the 3 axes as well as the total distance between the PET and CT positions were calculated for each point source.

Clinical imaging comparison with Discovery 710 PET/CT

A patient with local recurrence of nasal melanoma was referred to PET for follow-up after chemotherapy and radiation. The patient had a BMI of 24.2 and was injected with 3 MBq/kg for a total of 180 MBq ^{18}F-FDG. Ninety minutes after injection, a first TOF acquisition was made on a Discovery 710 PET/CT camera (GE Healthcare, Milwaukee, WI, USA). Two hundred minutes after injection, a second TOF acquisition was made on the Discovery MI 3-ring. The acquisition time at both systems was 13.5 min (1.5 min per bed position). Images were reconstructed using the Q.Clear algorithm, with a beta value of 400 for the Discovery 710 acquisition and 1000 for the Discovery MI 3 acquisition.

III. Results

Spatial resolution

Table 1,2 summarizes the spatial resolution results for VPHD re- construction algorithms. Here although the tangential resolution on the 3-ring system seemed somewhat better than on the 3-ring system comparing with other scanners. VPHD improved the spatial re- solution over by FBP, although statistical significance was only reached for FWHM in the axial direction and for FWTM in the tangential direction. As expected, VPHD combined with PSF modelling resulted in statistically better resolution than FBP and was also statistically better than VPHD, except for the FWHM radial resolution.

Table 1: Spatial resolution (FWHM & FWTM) in 3D mode at center (Point source position (cm) at 1cm radius using VPHD reconstruction

Description	3D Mode		Tolerance (mm)
	Measured (mm)	Reference (mm)	
FWHM in Radial Direction	3.84	≤ 5.1	≤ 1.05 of Reference
FWHM in Tangenital Direction	3.84	≤ 5.1	≤ 1.05 of Reference
FWHM in Axial Direction	4.18	≤ 5.6	≤ 1.05 of Reference
FWTM in Radial Direction	7.73	≤ 16.2	≤ 1.05 of Reference
FWTM in Tangenital Direction	7.98	≤ 16.2	≤ 1.05 of Reference
FWTM in Axial Direction	9.66	≤ 16.8	≤ 1.05 of Reference

Table 2: Spatial resolution (FWHM & FWTM) in 3D mode at center (Point source position (cm) at 10cm radius using VPHD reconstruction

Description	3D Mode		Tolerance (mm)
	Measured (mm)	Reference (mm)	
FWHM in Radial Direction	4.66	≤ 5.5	≤ 1.05 of Reference
FWHM in Tangenital Direction	4.08	≤ 6.5	≤ 1.05 of Reference
FWHM in Axial Direction	4.91	≤ 6.1	≤ 1.05 of Reference
FWTM in Radial Direction	8.67	≤ 16.5	≤ 1.05 of Reference
FWTM in Tangenital Direction	7.93	≤ 19.5	≤ 1.05 of Reference
FWTM in Axial Direction	9.55	≤ 18.3	≤ 1.05 of Reference

Sensitivity

The sensitivity at the centre of the FOV was 7.12 cps/kBq. The sensitivity at a radial offset of 10 cm from isocentre was 6.84 cps/kBq. Figure 1 shows the slice sensitivity profiles (cps/kBq) at 0 cm and 10cm [18].

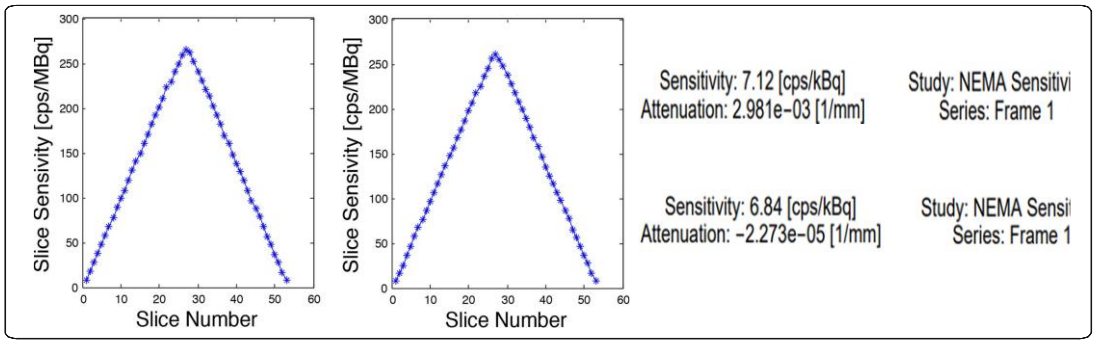

Fig. 1 Slice sensitivity profiles. The left panel shows the profile at the centre of the FOV (with 7.12 cps/kBq), the right panel is the profile at a 10-cm radial offset from isocentre (6.84 cps/kBq). As expected, the sensitivity is less than that of a 20-cm AFOV camera system (below).

Scatter fraction, count losses and Randoms

Figure 2 shows the total prompts, trues, randoms, scatters and NECR as a function of activity concentration. Figure 3 shows the scatter fraction as a function of activity concentration. Table 2 Peak NECR was 114.3 kcps; the activity concentration at this peak NECR was 22.2kBq/cc. Scatter fraction at peak NECR was 42.10%. The peak true counting rate on the MI 3 was 502.5 kcps at 29.5 kBq/ml.

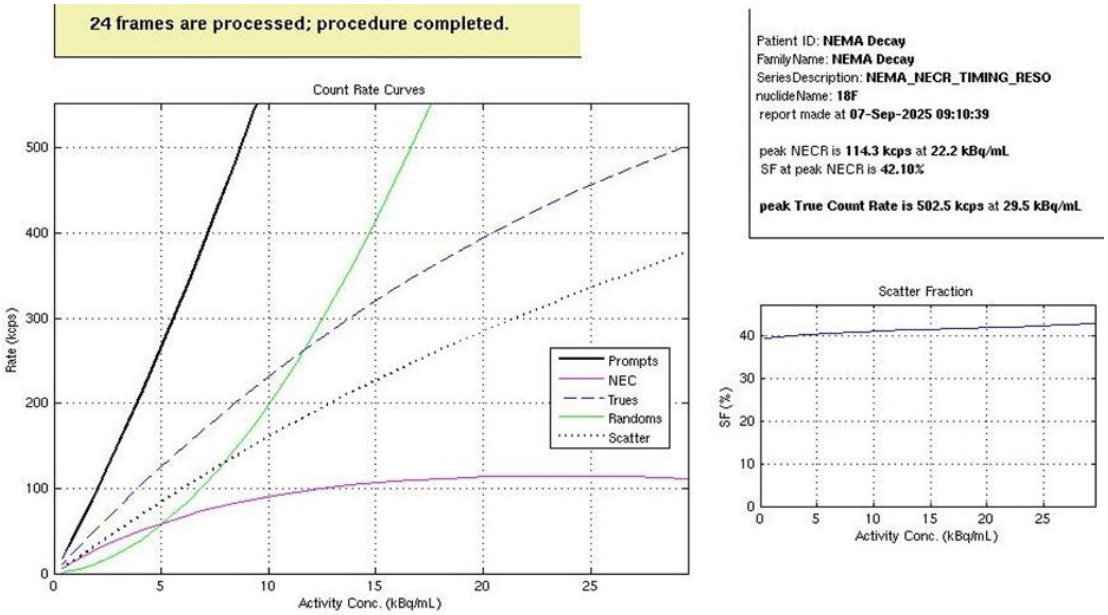

Fig. 2 Decay series—count rates as a function of activity concentration. Prompts, trues, randoms, scatters and NECR are depicted as a function of activity concentration. Peak NECR is 114.3 kcps at activity concentration of 22.2 kBq/mL. The peak true counting rate on the MI 3 was 502.5 kcps at 29.5 kBq/ml. NEC noise equivalent counts (below).

Accuracy: correction for count losses and randoms

Figure 4 shows, as a function of activity concentration, the minimum, maximum and mean error (%) of the measured image quantitation from the expected linear extrapolation from points below peak NECR. Notice that the errors are derived from reconstructed images to which all corrections have been applied, i.e. corrections for attenuation, randoms and scatter. Data points are shown for all activity concentrations probed during the decay series[18]. The maximum deviation from expected activity below peak NECR was 3.88%. For comparison, the maximum deviation on the Discovery MI 4-ring was 2.51% [3].

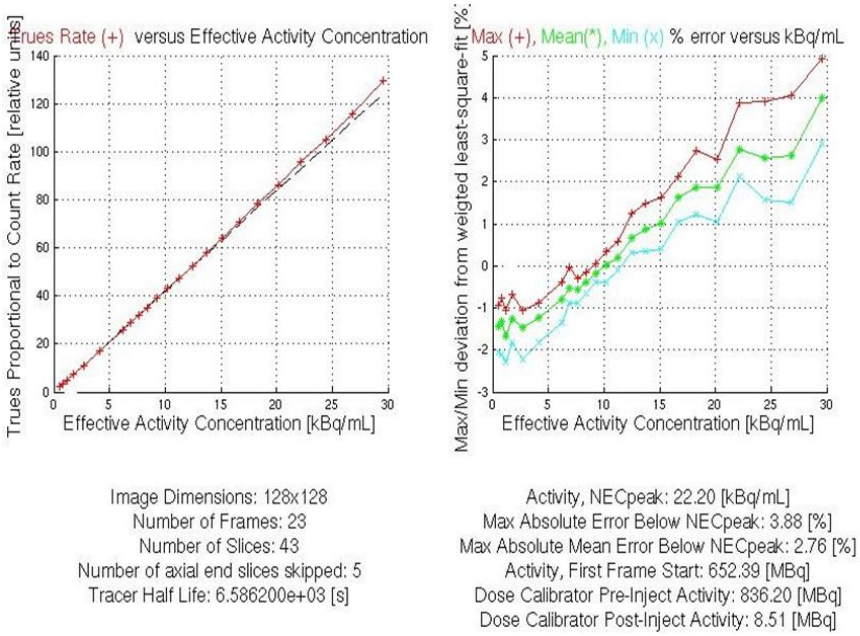

Fig. 3 Quantitation accuracy as a function of effective activity concentration. These errors are determined versus least squares fit of quantitation values below peak NECR. Maximal, minimal and mean absolute errors are given over all image slices except the 6 end slices on both ends of the AFOV (below).

IQ data according to NEMA NU2-2018. CR ranged from 96.2 % (smallest sphere) to 48.5% (largest sphere). BV ranged from 17.5% (smallest sphere) to 4.5% (largest sphere).

Image quality, attenuation accuracy and scatter correction

Table 4 shows Measures the accuracy of count losses and randoms corrections by comparing the trues rate calculated using count losses and randoms corrections with the trues rate extrapolated from measurements with negligible count losses and randoms. Documented measured values including other hospital with 4 ring GE PET CT, for comparing of variations[18].

Table 4 Counting rate data (NEMA-NU-2018)

Type of measurement	KAH 3 ring (this work)	Other Hospitals (4 ring)
Peak NECR (kcps)	114.3	185.7
Activity at peak NECR (kBq/ml)	22.2	21.7
Peak true counting rate[a] (kcps)	502.5	827.0
Activity at peak true counting rate[a] (kBq/ml)	29.5	34.8
Scatter fraction at peak NECR (%)	42.10	40.8
Max Absolute Error Below NEC peak	3.88	3.82

Timing and energy resolution

The average timing resolution was 411.2 ± 2.7 ps FWHM. Energy resolution was 9.94% ± 0.06% for the 3-ring detector. These results are very close to those obtained on the other 4-ring detector 410.4 ± 2.6 ps FWHM timing resolution and 9.84% ± 0.07% FWHM energy resolution[18].

PET/CT Co-registration accuracy

The accuracy measured between the PET and CT position in the form of max co-registration error for the three spheres sources were 17mm (0.1), 22mm (0.20), 28mm (20,0) The maximal co-registration error 1.69mm at 100cm[18].

Clinical imaging comparison with Discovery 710 PET/CT

Figure 4 shows maximal intensity projection images from the Discovery 710 and Discovery MI 3-ring PET/CT, reconstructed with the Q.Clear algorithm using beta values of 400 and 1000, respectively. In spite of one half-life of decay between the two studies, all lesions that were visible on the study performed on the Discovery 710 were also seen on the MI 3-ring study. Biodistribution changed somewhat between the two studies, with vascular activity diminishing and bowel and renal excretory activity increasing. Contrast improved on the later study in a left axillary node.

IV. Discussion

Spatial resolution on our 3-ring system overall was comparable to that on the 4-ring system and other commercially available systems. Iterative reconstruction without PSF correction introduces improvement over FBP as further iterating sharpens spatial resolution at the expense of image noise, although it should be acknowledged that the non-negativity constraint in iterative algorithms artificially enhances the apparent spatial resolution [26]. Nonetheless, additional PSF correction accomplished a major improvement due to the better modelling of the detector crystals response.

Scanner sensitivity was close to the value measured on the same system in [27]. It is better than for other systems with comparable FOV: 7.12 cps/kBq for the Discovery MI 3 ring with 15.0-cm axial FOV [13] and 6.53 cps/kBq for the Discovery 690/710 with an axial FOV of 15.7 cm [17] (Table 3). These values are all below those for systems with larger FOV [3, 27], as would be predicted from solid angle considerations, although of course other factors such as detector efficiency play a role as well in determining systems sensitivity. The peak *NECR* of the 3-ring system tested was close to the values measured on the same system in [27]. As expected, it is less than for other systems with larger FOV. The peak true counting rate and the activity at this rate presented in were FOV [27].

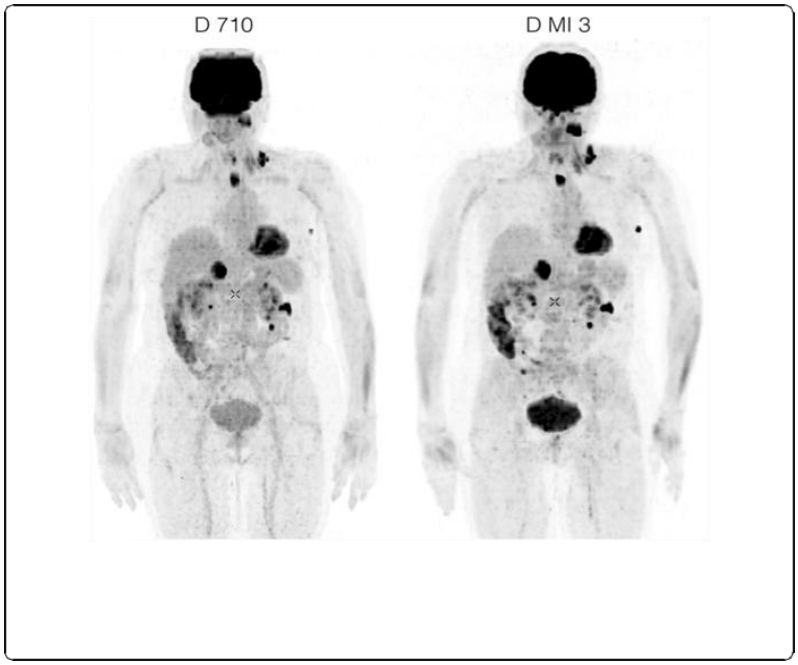

Fig. 4 Maximal intensity projection images. These were obtained in a melanoma patient on a Discovery 710 PET/CT (left panel) and, after one half-life radioactive decay, on a Discovery MI 3 PET/CT (right panel), using the same acquisition parameters. Image reconstruction by the Q.Clear algorithm used a beta value of 400 for the Discovery 710 acquisition and 1000 for the MI 3 acquisition. All lesions visible on the Discovery 710 study are visible on the Discovery MI 3 study as well

When a low beta value was used with the purpose of matching the noise level against VPFX reconstructed images, CR was enhanced by the Q.Clear reconstruction algorithm, similar to the 4-ring system [3]. Values on the 3-ring system using Q.Clear were higher than those on the 4-ring system using conventional TOF OSEM without PSF correction.

Background variability (table 4) with the 3-ring camera has been reported before the use extracted from the decay series at the first acquisition point, which is below the actual concentration needed to reach the trues peak. It was not deemed relevant to expose the operator to the high radiation levels that would be needed to explore a performance parameter irrelevant in clinical operations, considering the high photon sensitivity and low recommended clinical doses. The *quantitation accuracy* below the NEC peak of 3.88% only occurred at activity concentrations that are not clinically relevant.

Contrast recovery (table 3) as we measured the best of all systems reported [3]. For all hot spheres with concentration ratio of 21 kBq/cc (0.567μCi/cc) ^{18}F-FDG, called as hot spheres.

And the *timing resolution* of 411.2 ps nor the *energy resolution* of 9.94% was different from 4ring.

Co-registration accuracy of the PET CT was excellent with the maximal recorded error between the CT and PET coordinates being less than reference value i.e. less than 5.0mm for all point sources along all axes.

V. Conclusions

As expected from the smaller solid angle of the 3-ring camera, scanner sensitivity and NECR are lower and background variability is higher than those on the 4-ring digital camera system. Other NEMA specifications on the 3-ring digital PET/CT camera are all comparable to those on the 4-ring digital camera system. The SiPM-based PET may provide equal image quality within half of the acquisition time or with half the amount of tracer injected compared with a PET system based on vacuum photomultiplier tubes. Q.Clear reconstruction of the NEMA-IQ phantom with low beta values improves contrast recovery and diminishes background variability, when compared to images reconstructed with the manufacturer's recommended OSEM protocol.

Table 4 NEMA data on PET scanners available from our institution and Biograph mMR (PT/MR) collected from resources

Parameter	GE Healthcare		SIEMENS Healthcare	
	Discovery MI 3 PET/CT (this work)	Discovery 690/710 PET/CT (6)	Biograph mCT Flow PET/CT (9)	Biograph mMR PET/MR (16)
Axial FOV (cm)	15	15.7	22.1	25.8
Transverse FOV (cm)	70	70	70	59.4
Detector ring diameter (cm)	74.4	81	84.2	65.6
Crystal thickness (mm)	25	25	20	20
Spatial resolution FWHM (VPHD)				
Radial, 1 cm	3.84	4.52	4.22	4.3
Tangential, 1 cm	3.84	4.51	4.13	4.3
Axial, 1 cm	4.18	4.51	4.31	4.3
Radial, 10 cm	4.66	5.38	4.67	5.2
Tangential, 10 cm	4.08	4.81	4.92	4.8
Axial, 10 cm	4.91	5.74	5.09	6.6
Radial, 20 cm	7.15	NA	5.55	NA
Tangential, 20 cm	4.31	NA	6.48	NA
Axial, 20 cm	5.47	NA	7.8	NA
Sensitivity at centre of FOV (cps/kBq)	7.12	6.53	6.8	15
Counting rate statistics				
Peak NECR (kcps)	114.3	112.4	90.4	127.1
Peak NEC activity (kBq/ml)	22.2	29	19.9	50
Peak NEC scatter fraction (%)	42.1	38.78	36.4	30
Maximum absolute error NECpeak (%)	3.88	2.18	4.2	NA
Contrast recovery in spheres (VPHD)				
10 mm	47.4 (H)	44.5 (C)	33.99 (C)	32.5(C)
13 mm	61.2 (H)	69.1 (C)	42.12 (C)	50 (C)
17 mm	70.9 (H)	71 (C)	52.71 (C)	62.9 (C)
22 mm	77.5 (H)	85.4 (C)	59.69 (C)	70.8 (C)
28 mm	82.4 (H)	74.5 (C)	70.79 (C)	65.1 (C)
37 mm	88.1 (H)	84.1 (C)	77.91 (C)	72.3 (C)
Timing resolution (ps)	411.2	385.4	546.3	555
Energy resolution (%)	9.94	9.84	10.58	N/A

FOV field of view, FWHM full width at half maximum, FBP filtered back projection, NA not applicable, NEC(R) noise equivalent count (rate), [a] Radial and tangential FWHM, (H) Hot spheres, (C) Cold spheres.

Abbreviations

AFOV: Axial field of view; BV: Background variability; CR: Contrast recovery; CT: Computed tomography; FBP: Filtered backprojection; FDG: Fluorodeoxyglucose; FOV: Field of view; FWHM: Full width at half maximum; FWTM: Full width at tenth maximum; GE: General Electric; IQ: Image quality; LE: Lung error; MR(I): Magnetic resonance (imaging);
NEC(R): Noise equivalent count (rate); NEMA: National Electrical Manufacturers Association; OSEM: Ordered subset expectation maximization; PET: Positron-emission tomography; PSF: Point spread function; SiPM: Silicon photomultiplier; TOF: Time-of-flight; VPFX: Vue Point FX (= VPHD + TOF); VPHD: Vue Point HD (= OSEM), (H): Hot spheres, (C) Cold spheres.

Acknowledgements

Not applicable

Availability of data and materials

The phantom images are stored in the local database of the PET/CT system, in the Advantage Workstation AW-PET/CT on the nuclear medicine department and in the Advantage Workstation server in the imaging department of the hospital.

Authors' contributions

All authors contributed to the study design. Rasool kattubadi contributed to the acquisitions and processing. Hamad Almajid contributed in handling, data processing. Elmubarak Mohammadahmed in statistical data analysis during acceptance testing.

Authors' information

Rasool Kattubadi is an expert in nuclear medicine and medical radiation physics from the department of medical physics, King Abdulaziz Medical City, Riyadh, KSA. Hamad Almajid is an expert in nuclear medicine physics. Elmubarak Mohamedahmed is an expert in medical physics from the department of medical physics, King Abdulaziz Medical City, Riyadh, KSA.

Consent for publication

Not applicable.

Funding

This study was supported by King Abdulaziz Medical City, Riyadh, KSA

Data availability

The scanners and image data analyzed during the current study are available from the corresponding authors on reasonable request.

Declarations

Ethics approval and consent to participate: All procedures performed in studies involving human participants were in accordance with the ethical standards of the King Abdulaziz Medical City ethical committee and with the NEMA NU2 -2018 standards and informed consent was obtained from all individual participants included in the study.

Consent for publication

Not applicable.

Competing interests

The authors declare that they have no competing interests

References

[1]. Van Der Vos CS, Koopman D, Rijnsdorp S, Arends AJ, Boellaard R, Van Dalen JA, Et Al. Quantification, Improvement, And Harmonization Of Small Lesion Detection With State-Of-The-Art PET. Eur J Nucl Med Mol Imaging. 2017;44(Suppl 1):4–16.

[2]. Vandenberghe S, Mikhaylova E, D'Hoe E, Mollet P, Karp JS. Recent Developments In Time-Of-Flight PET. EJNMMI Phys. 2016;3:3.

[3]. Hsu DFC, Ilan E, Peterson WT, Uribe J, Lubberink M, Levin CS. Studies Of A Next Generation Silicon-Photomultiplier-Based Time-Of-Flight PET/CT System. J Nucl Med. 2017;58:1511–8.

[4]. National Electrical Manufacturers Association. NEMA NU-2-2012 Performance Measurement Of Positron Emission Tomographs. Rosslyn: National Electrical Manufacturers Association; 2013.

[5]. De Ponti E, Morzenti S, Guerra L, Pasquali C, Arosio M, Bettinardi V, Et Al. Performance Measurements For The PET/CT Discovery-600 Using NEMA NU 2-2007 Standards. Med Phys. 2011;38:968–74.

[6]. Bettinardi V, Presotto L, Rapisarda E, Picchio M, Gianolli L, Gilardi MC. Physical Performance Of The New Hybrid PETCT Discovery-690. Med Phys. 2011;38:5394–411.

[7]. Martí-Climent JM, Prieto E, Domínguez-Prado I, García-Velloso MJ, Rodríguez-Fraile M, Arbizu J, Et Al. Contribution Of Time Of Flight And Point Spread Function Modeling To The Performance Characteristics Of The PET/CT Biograph Mct Scanner. Rev Esp Med Nucl Imagen Mol. 2013;32:13–21.

[8]. Jakoby BW, Bercier Y, Conti M, Casey ME, Bendriem B, Townsend DW. Physical And Clinical Performance Of The Mct Time-Of-Flight PET/CT Scanner. Phys Med Biol. 2011;56:2375–89.

[9]. Rausch I, Cal-González J, Dapra D, Gallowitsch HJ, Lind P, Beyer T, Et Al. Performance Evaluation Of The Biograph Mct Flow PET/CT System According To The NEMA NU2-2012 Standard. EJNMMI Phys. 2015;2:26.

[10]. Kolthammer JA, Su KH, Grover A, Narayanan M, Jordan DW, Muzic RF. Performance Evaluation Of The Ingenuity TF PET/ CT Scanner With A Focus On High Count-Rate Conditions. Phys Med Biol. 2014;21(59):3843–59.

[11]. Surti S, Kuhn A, Werner ME, Perkins AE, Kolthammer J, Karp JS. Performance Of Philips Gemini TF PET/CT Scanner With Special Consideration For Its Time-Of-Flight Imaging Capabilities. J Nucl Med. 2007;48:471–80.

[12]. Grogg KS, Toole T, Ouyang J, Zhu X, Normandin MD, Li Q, Et Al. National Electrical Manufacturers Association And Clinical Evaluation Of A Novel Brain PET/CT Scanner. J Nucl Med. 2016;57:646–52.

[13]. Akamatsu G, Uba K, Taniguchi T, Mitsumoto K, Narisue A, Tsutsui Y, Et Al. Impact Of Time-Of-Flight PET/CT With A Large Axial Field Of View For Reducing Whole-Body Acquisition Time. J Nucl Med Technol. 2014;42:101–4.
[14]. Grant AM, Deller TW, Khalighi MM, Maramraju SH, Delso G, Levin CS. NEMA NU 2-2012 Performance Studies For The Sipm-Based Tof-PET Component Of The GE SIGNA PET/MR System. Med Phys. 2016;43:2334.
[15]. Karlberg AM, Sæther O, Eikenes L, Goa PE. Quantitative Comparison Of PET Performance-Siemens Biograph Mct And Mmr. EJNMMI Phys. 2016;3:5.
[16]. Delso G, Fürst S, Jakoby B, Ladebeck R, Ganter C, Nekolla SG, Et Al. Performance Measurements Of The Siemens Mmr Integrated Whole-Body PET/MR Scanner. J Nucl Med. 2011;52:1914–22.
[17]. Miller M, Zhang J, Binzel K, Griesmer J, Laurence T, Narayanan M, Et Al. Characterization Of The Vereos Digital Photon Counting PET System. J Nucl Med. 2015;56(Suppl. 3):434.
[18]. National Electrical Manufacturers Association. NEMA NU-2-2018 Performance Measurement Of Positron Emission Tomographs. Rosslyn: National Electrical Manufacturers Association; 2018.
[19]. Nuyts J, Bequé D, Dupont P, Mortelmans L. A Concave Prior Penalizing Relative Differences For Maximum-A-Posteriori Reconstruction In Emission Tomography. IEEE Trans Nucl Sci. 2002;49:56–60.
[20]. Ahn S, Fessier JA. Globally Convergent Image Reconstruction For Emission Tomography Using Relaxed Ordered Subsets Algorithms. IEEE Trans Med Imaging. 2003;22:613–26.
[21]. Ross S. Q.Clear. GE Healthcare White Paper. 2014. Https://Www.Gehealthcare.Com/-/Media/739d885baa59485aaef5ac0e0eeb44a4.Pdf. Accessed 4 May 2019.
[22]. Teoh EJ, Mcgowan DR, Macpherson RE, Bradley KM, Gleeson FV. Phantom And Clinical Evaluation Of The Bayesian Penalized Likelihood Reconstruction Algorithm Q.Clear On An LYSO PET/CT System. J Nucl Med. 2015;56:1447–52.
[23]. Teoh EJ, Mcgowan DR, Bradley KM, Belcher E, Black E, Gleeson FV. Novel Penalised Likelihood Reconstruction Of PET In The Assessment Of Histologically Verified Small Pulmonary Nodules. Eur Radiol. 2016;26:576–84.
[24]. Rowley LM, Bradley KM, Boardman P, Hallam A, Mcgowan DR. Optimization Of Image Reconstruction For (90)Y Selective Internal Radiotherapy On A Lutetium Yttrium Orthosilicate PET/CT System Using A Bayesian Penalized Likelihood Reconstruction Algorithm. J Nucl Med. 2017;58:658–64.
[25]. Sah BR, Stolzmann P, Delso G, Wollenweber SD, Hüllner M, Hakami YA, Et Al. Clinical Evaluation Of A Block Sequential Regularized Expectation Maximization Reconstruction Algorithm In 18F-FDG PET/CT Studies. Nucl Med Commun. 2017;38:57–66.
[26]. Gong K, Cherry SR, Qi J. On The Assessment Of Spatial Resolution Of PET Systems With Iterative Image Reconstruction. Phys Med Biol. 2016;61:N193–202.
[27]. Levin C, Peterson W, Ross S, Stearns C, Uribe J. PET Performance As A Function Of Axial Field Of View For A New Silicon Photomultiplier-Based Whole Body TOF PET/CT System. J Nucl Med. 2016;57(Suppl. 2):200.